Applied Catalysis B: Environmental 256 (2019) 117801

Contents lists available at ScienceDirect

Applied Catalysis B: Environmental

journal homepage: www.elsevier.com/locate/apcatb

On the design and operation of solar photo-Fenton open reactors for the removal of contaminants of emerging concern from WWTP effluents at neutral pH

P. Soriano-Molina[a,b], J.L. García Sánchez[a,b], S. Malato[a,c], P. Plaza-Bolaños[a], A. Agüera[a], J.A. Sánchez Pérez[a,b,*]

[a] Solar Energy Research Centre (CIESOL), Joint Centre University of Almería-CIEMAT, Carretera de Sacramento s/n, E-04120, Almería, Spain
[b] Chemical Engineering Department, University of Almería, Ctra de Sacramento s/n, E-04120, Almería, Spain
[c] Plataforma Solar de Almería, CIEMAT, Carretera Senés Km. 4, E-04200, Tabernas, Almería, Spain

ARTICLE INFO

Keywords:
Advanced oxidation process
EDDS
Microcontaminant
Raceway pond reactor
Wastewater

ABSTRACT

This work presents for the first time a tool for the design of continuous raceway pond reactors to remove contaminants of emerging concern (CECs) from WWTP secondary effluents by solar photo-Fenton process at neutral pH. The effects of the hydraulic residence time (HRT) and the liquid depth on the treatment capacity were studied, the availability of solar UV radiation being the main environmental variable. Treatment capacities as high as 1800 and 9000 L m^{-2} d^{-1} were estimated for 70% CEC removal in winter and summer, respectively. To this aim, the performance of a kinetic model of the photo-Fenton process developed with Fe^{3+}-EDDS was updated to predict CEC removal in effluents collected from different WWTPs. To reach a goal of CEC elimination, the treatment capacity can be maximized as a function of HRT and liquid depth, and consequently the reactor surface area is calculated to treat a given flow rate.

1. Introduction

The development of anthropogenic activities, such as agriculture or chemical and pharmaceutical industry, has brought along the production of different chemical compounds including personal care products, pharmaceuticals, hormones or pesticides. Currently, they are known as contaminants of emerging concern (CECs), since they are considered as a potential threat to the environment and biota [1,2]. One of the main sources of CECs are effluents from conventional wastewater treatment plants (WWTPs), which are not designed to remove these compounds, and consequently a high proportion of them are discharged to the aquatic environment. Although the discharge of CECs has not been regulated yet, rules in Switzerland demand 80% removal efficiency of total load of CECs with respect to raw wastewater [3]. Furthermore, the Commission Decision 2015/495/EU provides a list of 17 CECs to be monitored in the European Union (EU) [4]. Consequently, there is a global interest in the development of tertiary treatments for the removal of these compounds in municipal WWTPs (MWWTPs) [5]. The oxidation conditions used to achieve this goal does not enhance mineralization of wastewater, since CECs only represent a hundredth part of the total organic content. Among these treatments, solar photo-Fenton has been demonstrated to be an environmentally friendly and highly efficient advanced oxidation process (AOP) [6,7].

Nowadays, the research is focused on the operation of the process at neutral pH to deal with the drawbacks of the conventional photo-Fenton process at acidic pH, reducing operating cost and avoiding the increase in the salinity of the effluents. To maintain iron in solution, the use of chelating agents such as ethylenediamine-*N,N'*-disuccinic acid (EDDS) has been proposed [8]. The removal of CECs by photo-Fenton with Fe^{3+}-EDDS has been widely demonstrated in synthetic and real effluents [9–11]. A recent work shows that high removal efficiencies of around 80% can be achieved in real effluents of very different composition by the process operated at neutral pH with Fe^{3+}-EDDS [12]. In addition, recent studies point out that the toxicity of the wastewater is reduced after photo-Fenton treatment with Fe^{3+}-EDDS [10,13].

Once the process efficiency is demonstrated, it is important to study the reaction mechanisms for further development of models to control and optimize the treatment. Wastewater composition, irradiance, reactant concentration as well as reactor geometry are the variables that most affect the kinetics of the process [14]. Therefore, they must be considered for the design of treatment plants. Regarding the photo-Fenton process, there are few models reported for CEC removal.

* Corresponding author at: Department of Chemical Engineering, University of Almería, 04120, Almería, Spain.
E-mail address: jsanchez@ual.es (J.A. Sánchez Pérez).

https://doi.org/10.1016/j.apcatb.2019.117801
Received 12 April 2019; Received in revised form 29 May 2019; Accepted 30 May 2019
Available online 05 June 2019
0926-3373/

Schenone et al. [15] proposed a model for the degradation of the herbicide 2,4-dichlorophenoxyacetic (2,4-D) at circumneutral pH using ferrioxalate complex. Giannakis et al. [16] developed a strategy to optimize the operating range concerning the reagents and pH by using the Response Surface methodology. In a recent work, a mechanistic modeling of the process with Fe^{3+}-EDDS has been obtained and successfully validated outdoors in a low-cost RPRs with simulated secondary effluent [17].

These models have been developed under controlled conditions, in demineralized water or synthetic wastewater. The experimental results may differ greatly from the predicted results when applying the models in real conditions, since the reaction mechanisms are affected by variations in WWTP effluent composition. Inorganic ions such as chlorides, sulfates and bicarbonates can substantially affect CEC removal [18,19]. Moreover, author's recent work carried out in secondary effluents from different MWWTPs shows that the nature of organic matter has a great effect on the kinetics of the process [12].

Therefore, extending the application of mechanistic models of solar photo-Fenton to cover CEC removal in real MWWTP effluents of very different composition would be desirable. In order to maximize the treatment capacity of a treatment plant, it is very important to evaluate the performance of models and its degree of adaptability to different perturbations under different operating conditions. To this aim, this paper presents for the first time a design tool for the real treatment of MWWTP effluents by solar photo-Fenton. The kinetic model recently reported for photo-Fenton process with Fe^{3+}-EDDS [17] was applied to the experimental results obtained in secondary effluents collected from five MWWTPs. The model was further validated for the operation of RPRs in continuous flow mode. The hydraulic residence time (HRT) and the liquid depth in RPRs were the operating variables, whereas the solar UV radiation was the external uncontrollable variable. Meanwhile, maximizing the treatment capacity in terms of volume of water treated per unit of reactor surface area and time (L m^{-2} d^{-1}) was the design target. The three most abundant CECs detected in secondary effluents from five MWWTPs were selected as target compounds (*O*-desmethyltramadol (O-DSMT*)* and *O*-desmethylvenlafaxine (O-DSMV) and gabapentin (GBP)). These compounds are drugs or their metabolites (tramadol and venlafaxine) commonly used and highly persistent to conventional treatments, and consequently, they are being detected at high concentrations in MWWTPs located in different countries [20–23].

2. Experimental

2.1. Chemicals

Hydrogen peroxide (33%, w/v), ferric sulfate hydrate (75%, w/w), acetic acid (99.7%, w/v), 1,10-phenantroline (99%, w/w) and hydrochloric acid (37%, w/v) were supplied by Panreac (Barcelona, Spain). Methanol (MeOH) and acetonitrile were high pressure liquid chromatography (HPLC) grade and acquired from Sigma-Aldrich (Steinheim, Germany). Sodium formate (99% w/w) was obtained from Merck Millipore (Darmstadt, Germany). Ultrapure water was produced with a Millipore Direct-Q® Ultrapure Water System (Bedford, MA, USA). Formic acid (95%, w/v), sulfuric acid (95%, w/v), tetrabutylammonium bisulfate (97%, w/w), titanium (IV) oxysulfate (1.9%, w/v), ascorbic acid (99%, w/w), EDDS (35%, w/v) and high purity analytical standards were supplied by Sigma-Aldrich.

2.2. Chemical analysis

The concentration of H_2O_2 was determined by the spectrophotometric method DIN 38 402 H15, whereas total dissolved iron concentration was measured according to the 1,10-phenanthroline (ISO 6332) colorimetric procedure. The limits of quantification (LOQs) were 6.1 10^{-4} mM and 4.5 10^{-3} mM, respectively.

The concentration of Fe^{3+}-EDDS was determined by ultrahigh-pressure liquid chromatography with diode array detection (UHPLC-DAD) in an Agilent Technologies 1200 Series instrument (Waldbronn, Germany). Isocratic elution was applied, using a mobile phase composed of 5% of MeOH and 95% of 2 mM tetrabutylamonium hydrogen sulfate and 15 mM sodium formate in water [24]. The flow was 0.5 mL min^{-1}. The LOQ was 3.5 10^{-3} mM.

The direct injection technique was used to determine the concentration of CECs by high-performance liquid chromatography quadrupole-linear ion trap analyzer (LC-QqLIT-MS/MS); further details can be found elsewhere [25].

Dissolved organic carbon (DOC) and inorganic carbon (IC) were quantified with a Shimadzu-V CPH TOC analyzer (Shimadzu Corporation, Kyoto, Japan). The LOQ was 1 mg L^{-1}.

The concentration of anions was measured using ion chromatography Metrohm 881 Compact IC pro (Herisau, Switzerland). The eluent consisted of a solution of 3.6 mM Na_2CO_3 with flow rate of 0.8 mL min^{-1}.

2.3. Experimental set-up

The experiments were carried outdoors at the Solar Energy Research Center (CIESOL) located at the University of Almeria (Andalusia, Spain) in RPRs. This type of photoreactor consists of a pond divided in two channels with a paddlewheel to maintain an uniformly mixed flow [26]. The RPRs were made of PVC with 5 and 15 cm liquid depth, respectively (19-L and 78-L capacity), Fig. 1. Wastewater temperature and natural pH were in the range 22–26 °C and 7–8, respectively. Both variables were measured online with sensors connected to a LabJack USB/Ethernet data logging device. The concentration of H_2O_2 and Fe^{3+} (at a Fe^{3+}-EDDS molar ratio of 1:1) were set at 0.88 mM (30 mg L^{-1}) and 0.1 mM (5.6 mg L^{-1}), respectively. These are the optimal conditions reported for the photo-Fenton process in this type of reactor for CEC removal [12].

For modeling purposes, UV irradiance in Almeria city (36°50´17´´N, 2°27´35´´W) was estimated using the software SMARTS2 (version 2.9.5, Florida, USA) [27]. This software allows to estimate the spectral distribution of solar radiation, both direct and diffuse components, from spectral transmittance functions for the main extinction processes in the atmosphere. These data were corroborated with the experimental measurements obtained with a solar global UV radiometer (LPUVA02AV, Delta Ohm, Padua, Italy), the spectral response being in the range 327–384 nm.

In this paper, a recently published mechanistic model for solar photo-Fenton process with Fe^{3+}-EDDS [17] has been applied to the experimental data of CEC removal in effluents from different MWWTPs. Experiments to obtain the model parameters were carried out in a 5-cm deep RPR operated in batch mode [12]. The MWWTP effluents were classified according to the criteria established in a previous publication [12]. Thus, the resulting classification was as follows: high-level (effluent from El Ejido, Almeria, Spain), medium-level A (effluent from El

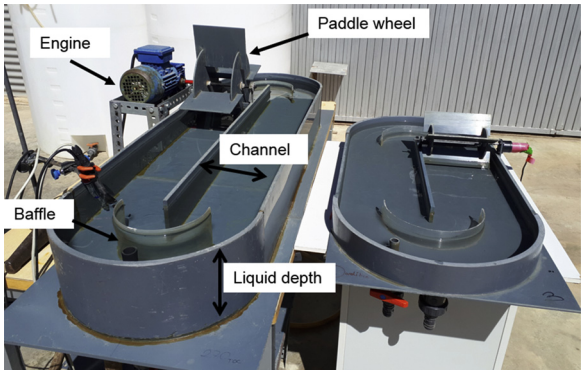

Fig. 1. 5-cm (right) and 15-cm (left) deep RPRs.

Bobar, Almeria, Spain), medium-level B (effluent from El Toyo, Almeria, Spain), low-level A (effluent from Girona, Spain), low-level B (effluent from Alcoy, Alicante, Spain). Further details about the MWWTPs and the characterization of effluents were previously reported [12].

Once the model parameters were obtained, the model was validated by predicting CEC removal for the operation of RPRs in continuous flow mode. In this regard, continuous flow experiments were conducted with medium-level B effluent (see Table S1) in RPRs of 5 and 15 cm liquid depth at two HRTs. The assays were performed as follows:

Firstly, the reactors were operated in batch mode for 30 min, until Fe^{3+}-EDDS photo-decomposition. Then, both reactant and wastewater supply pumps were turned on and the process was performed in continuous flow mode. The 5-cm deep RPR was operated with a 15-min HRT (1.27 L min^{-1} total flow rate) for 120 min. Then, the flow rate was increased, and the process was performed with a 10-min HRT (1.90 L min^{-1}) for 120 min. As for the experiment in 15-cm deep RPR, the reactor was operated with a 30-min HRT (2.60 L min^{-1} total flow rate) for 180 min. Then, the flow rate was increased, and the reaction was carried out with a 20-min HRT (3.90 L min^{-1} total flow rate) for 120 min.

3. Parameter estimation of the Fe^{3+}-EDDS photo-Fenton kinetic model for real secondary effluents

The target CECs to fit the model were the metabolite of the opioid tramadol, O-DSMT (319–1976 ng L^{-1}), the metabolite of the pharmaceutical venlafaxine, O-DSMV (684–1325 ng L^{-1}) and the pharmaceutical GBP (943–7863 ng L^{-1}). The range shown in parenthesis corresponds to the five effluents assayed. The reaction mechanism above referred is shown in Table 1.

The kinetic parameters were determined from the experimental data previously obtained in the different MWWTP effluents operating the 5-cm deep RPR in batch mode. To this end, the built-in functions of the MATLAB optimization toolbox were used, the objective function being the minimization of the squared errors between experimental data and model estimation for the set of measured variables, Eq. (1). In this expression, p refers to the number of experimental conditions used (p = 2), n is the number of data point in each assay, (n = 8). G, T, V, H and F denote GBP, O-DSMT, O-DSMV, H_2O_2 and Fe^{3+}-EDDS concentration, respectively. Subscript m stands for model data and x experimental data.

$$J = \sum_{j=1}^{p}\left[\sum_{i=1}^{n}\left(\frac{G_{x(i,j)}-G_{m(i,j)}}{G_{x(1,j)}}\right)^2+\left(\frac{T_{x(i,j)}-T_{m(i,j)}}{T_{x(1,j)}}\right)^2+\left(\frac{V_{x(i,j)}-V_{m(i,j)}}{V_{x(1,j)}}\right)^2+\left(\frac{H_{x(i,j)}-H_{m(i,j)}}{H_{x(1,j)}}\right)^2+\left(\frac{F_{x(i,j)}-F_{m(i,j)}}{F_{x(1,j)}}\right)^2\right] \quad (1)$$

Due to the variability in the experimental results obtained in each MWWTP effluent, the search for parameters was carried out separately for each type of effluent. Table 2 shows the kinetic constants obtained for each type of effluent.

The kinetic constants corresponding to the Fenton reaction, R. (6), as well as the oxidation of IC and H_2O_2 with $HO^{\bullet}$, R. (13) and R. (14), were taken from the literature ($k_6 = 4.56\ mM^{-1}\ min^{-1}$ [28], $k_{13} = 5.1{\cdot}10^5\ mM^{-1}\ min^{-1}$, $k_{14} = 1.6{\cdot}10^6\ mM^{-1}\ min^{-1}$ [29]). As it can be observed, they are of the same order of magnitude in the five effluents. Briefly, k_3 is much higher than k_2 in all the effluents, which points out that most of the energy absorbed by Fe^{3+}-EDDS is used in its reduction, whereas a small fraction of energy is released as heat (Q). However, k_{10} ($[Fe^{3+}{-}EDDS_{ox}]^*$ deactivation) is higher than k_{11} ($[Fe^{3+}{-}EDDS_{ox}]^*$ photoreduction) which is explained by the lower

Table 2
Model parameters estimated in each MWWTP effluent.

Kinetic constant	High-Level	Medium-Level A	Medium-Level B	Low-Level A	Low-Level B
k_2 (min^{-1})	0.65	0.65	0.69	0.57	0.45
k_3 (min^{-1})	15.79	7.40	17.52	20.66	17.35
k_4 ($mM^{-1}\ min^{-1}$)	$1.2{\cdot}10^3$	$1.0{\cdot}10^3$	$1.7{\cdot}10^3$	$1.2{\cdot}10^3$	$1.3{\cdot}10^3$
k_5 (min^{-1})	37.66	48.27	59.28	39.82	45.23
k_7 ($mM^{-1}\ min^{-1}$)	0.13	0.10	0.14	0.19	0.23
k_8 ($mM^{-1}\ min^{-1}$)	$3.6{\cdot}10^7$	$5.1{\cdot}10^7$	$3.9{\cdot}10^7$	$5.0{\cdot}10^7$	$4.9{\cdot}10^7$
k_{10} (min^{-1})	11.30	49.60	15.94	15.72	20.86
k_{11} (min^{-1})	3.25	1.02	2.95	1.70	1.36
k_{12} ($mM^{-1}\ min^{-1}$)	$5.6{\cdot}10^6$	$2.9{\cdot}10^6$	$3.9{\cdot}10^6$	$7.0{\cdot}10^6$	$3.8{\cdot}10^6$
k_{15} ($mM^{-1}\ min^{-1}$)	$2.2{\cdot}10^6$	$1.3{\cdot}10^6$	$2.2{\cdot}10^6$	$3.4{\cdot}10^6$	$3.7{\cdot}10^6$
k_{16} ($mM^{-1}\ min^{-1}$)	$7.5{\cdot}10^7$	$2.3{\cdot}10^7$	$8.8{\cdot}10^7$	$5.6{\cdot}10^7$	$5.0{\cdot}10^7$
k_{17} ($mM^{-1}\ min^{-1}$)	$7.7{\cdot}10^7$	$1.7{\cdot}10^7$	$7.9{\cdot}10^7$	$5.8{\cdot}10^7$	$4.4{\cdot}10^7$
k_{18} ($mM^{-1}\ min^{-1}$)	$6.8{\cdot}10^7$	$1.1{\cdot}10^7$	$5.1{\cdot}10^7$	$2.2{\cdot}10^7$	$3.6{\cdot}10^7$

Table 1
Model reactions and rate law equations.

Reaction	Rate equation	Reaction number
$Fe^{3+}-EDDS+ h\upsilon \rightarrow [Fe^{3+}-EDDS]^*$	$r_1 = VRPA_1^h$	R. (1)
$[Fe^{3+}-EDDS]^* \rightarrow Fe^{3+}-EDDS+ Q$	$r_2 = k_2\,[[Fe^{3+}{-}EDDS]^{-*}]$	R. (2)
$[Fe^{3+}-EDDS]^* \rightarrow Fe^{2+}-EDDS+ H^+$	$r_3 = k_3\,[[Fe^{3+}{-}EDDS]^{-*}]$	R. (3)
$Fe^{2+}-EDDS+ H_2O_2 \rightarrow Fe^{3+}-EDDS+ HO^{\bullet} + HO^-$	$r_4 = k_4\,[Fe^{2+}{-}EDDS]\,[H_2O_2]$	R. (4)
$Fe^{2+}-EDDS \rightarrow Fe^{2+} + EDDS^{\bullet 3-}$	$r_5 = k_5\,[Fe^{2+}{-}EDDS]$	R. (5)
$Fe^{2+} + H_2O_2 \rightarrow Fe(OH)_3 + HO^{\bullet} + HO^-$	$r_6 = k_6\,[Fe^{2+}]\,[H_2O_2]$	R. (6)
$Fe^{3+}-EDDS+ H_2O_2 \rightarrow Fe^{2+}-EDDS+ O_2^{\bullet -} + 2H^+$	$r_7 = k_7\,[[Fe^{3+}{-}EDDS]^-]\,[H_2O_2]$	R. (7)
$Fe^{3+}-EDDS+ HO^{\bullet} \rightarrow Fe^{3+}{-}EDDS_{ox}$	$r_8 = k_8\,[[Fe^{3+}{-}EDDS]^-]\,[HO^{\bullet}]$	R. (8)
$Fe^{3+}{-}EDDS_{ox} + h\upsilon \rightarrow [Fe^{3+}{-}EDDS_{ox}]^*$	$r_9 = VRPA_2^i$	R. (9)
$[Fe^{3+}{-}EDDS_{ox}]^* \rightarrow Fe^{3+}{-}EDDS_{ox} + heat$	$r_{10} = k_{10}\,[[Fe^{3+}-EDDS_{ox}]^*]$	R. (10)
$[Fe^{3+}{-}EDDS_{ox}]^* \rightarrow Fe^{2+} + EDDS^{\bullet 3-}$	$r_{11} = k_{11}\,[[Fe^{3+}-EDDS_{ox}]^*]$	R. (11)
$OM^a + HO^{\bullet} \rightarrow MX^b$	$r_{12} = k_{12}\,[MO]\,[HO^{\bullet}]$	R. (12)
$IC^c + HO^{\bullet} \rightarrow ICX^d$	$r_{13} = k_{13}\,[IC]\,[HO^{\bullet}]$	R. (13)
$H_2O_2 + HO^{\bullet} \rightarrow 2H_2O + O_2$	$r_{14} = k_{14}\,[H_2O_2]\,[HO^{\bullet}]$	R. (14)
$EDDS^{\bullet 3-} + H_2O_2 \rightarrow 10MX$	$r_{15} = k_{15}\,[H_2O_2]\,[EDDS^{\bullet 3-}]$	R. (15)
$O{-}\ DSMT^e + HO^{\bullet} \rightarrow 15MX$	$r_{16} = k_{16}\,[O{-}\ DSMT]\,[HO^{\bullet}]$	R. (16)
$O{-}\ DSMV^f + HO^{\bullet} \rightarrow 16MX$	$r_{17} = k_{17}\,[O{-}\ DSMV]\,[HO^{\bullet}]$	R. (17)
$GBP^g + HO^{\bullet} \rightarrow 9MX$	$r_{18} = k_{18}\,[GBP]\,[HO^{\bullet}]$	R. (18)

[a]Organic matter; [b]Oxidized organic matter; [c]Inorganic carbon; [d]Oxidized inorganic carbon; [e]*O*-Desmethyltramadol; [f]*O*-Desmethylvenlafaxine; [g]Gabapentin; [h]Volumetric rate of photon absorption of Fe^{3+}-EDDS; [i]Volumetric rate of photon absorption of Fe^{3+}-$EDDS_{ox}$.

Table 3
Root mean squared errors between experimental data and model predictions.

Compound	High-level	Medium-level A	Medium-level B	Low-level A	Low-level B
Fe^{3+}-EDDS	3.9	5.6	2.9	2.1	3.9
H_2O_2	6.3	5.0	8.2	2.8	5.2
O-DSMT[a]	2.9	3.9	4.1	4.4	3.7
O-DSMV[b]	4.0	6.3	4.8	5.5	3.3
GBP[c]	3.7	4.2	4.0	4.3	2.2

[a] *O*-Desmethyltramadol.
[b] *O*-Desmethylvenlafaxine.
[c] Gabapentin.

quantum efficiency of the complex after being oxidized. The kinetic constant corresponding to Fe^{2+}-EDDS oxidation with $HO^{\bullet}$, k_4, is three orders of magnitude higher than the kinetic constant for the classic Fenton, k_6. All these observations are in concordance with the kinetic model reported for synthetic effluent [17]. Comparing the kinetic constants for CEC oxidation (k_{16}, k_{17} and k_{18}), differences between the effluents are not directly related to their salinity, in concordance with the previous observation that CEC removal could be mainly affected by the composition of the organic matter present in the effluent. In medium-level A, the values corresponding to the oxidation of the three CECs are lower than in the rest of effluents. This agrees with the values of the pseudo-first order rate constants reported for the removal of total load of CECs in these effluents [12].

The model successfully fits experimental data of all the measured species, both the consumption of reagents and the kinetics of the CEC removal. The quality of the fit computed through the root mean square error (RMSE) equation is shown in Table 3. The highest RMSE values were 5.6%, 8.2%, 4.4%, 6.3% and 4.3% for Fe^{3+}-EDDS, H_2O_2, O-DSMT and O-DSMV and GBP, respectively. As an example, Fig. 2 shows the reactant consumption as well as the CEC profiles in high-level and low-level A effluents.

The obtained results show that the model for the photo-Fenton process previously proposed (which was developed under controlled conditions and synthetic wastewater) can be tuned to predict the kinetic of CEC removal in real municipal WWTP effluents, these compounds being in concentrations in the range from few μg L^{-1} to hundreds of ng L^{-1}. Therefore, the model could be a useful tool for the control and optimization of the process in MWWTPs.

4. Results and discussion

4.1. Kinetic model validation in continuous flow operation

When operating the solar photo-Fenton process with Fe^{3+}-EDDS the reaction times are short (lower than 30 min). At such a short reaction time, the reactor should be operated in continuous flow on a larger scale, as previously reported [11,12]. In this way, the treatment capacity is increased, and the costs associated with charge and discharge operations are avoided. To validate the capability of the model to predict CEC removal when operating RPRs in continuous flow mode, the kinetic parameters estimated for medium-level B effluent were selected. The mass balances in continuous flow for the species shown in Table 1, are shown in Table 4. Q_F, Q_H and Q_W ($m^3\ min^{-1}$) stand for the incoming flow rate of Fe^{3+}-EDDS, H_2O_2 and wastewater, respectively; Q_S ($m^3\ min^{-1}$) is the outgoing flow rate; V (m^3) is the reaction volume; and e denotes inlet stream. Constant volume in continuous operation is set by overflow and so the outgoing flow rate is defined by Eq. (2):

$$Q_S = Q_H + Q_W + Q_F \quad (2)$$

The set of mass balances was solved with MATLAB. The input variables were the flow rates (both of reactant and wastewater supply pumps), the liquid depth, the irradiance, and the concentration of the different species in the feed tanks. As mentioned in Section 2, each reactor was operated varying the HRT (15 and 10 min for 5-cm deep RPR and 30 and 20 min for 15-cm deep RPR). In all cases, reactant concentrations added to the reactor were 0.88 mM H_2O_2 and 0.1 mM Fe^{3+} at Fe^{3+}-EDDS molar ratio of 1:1.

Fig. 3 shows a comparison between model predictions and experimental data obtained for 5-cm and 15-cm liquid depth, respectively. Once the operation in continuous flow mode was started, the concentration of reactant and CECs increased up to the steady state, it being reached after 20 min. On the other hand, the concentration of Fe^{3+}-EDDS and H_2O_2 increased when the HRT was decreased. Nonetheless, this effect was less significant in CEC profiles, the average removal percentages (with respect to the sum of the three CECs) being 78% and 76% in 5-cm RPR with 15 and 10-min HRT, respectively. In the 15-cm RPR, the removal percentages were 87% and 82% with 30 min and 20-min HRT, respectively.

Concerning the experiment in the 5-cm RPR, the model successfully predicts experimental data for both the reactant consumption and the CECs. When operating the process at solar noon (assay at 15-min HRT), their respective concentrations remained constant at the value corresponding to the steady state. However, the plateau corresponding to the steady state is not observed at 10-min HRT, the concentration being increased over the course of the process. This is due to the experiment was conducted after solar noon, and consequently UV radiation decreased. This effect is clearly observed in Fe^{3+}-EDDS concentration, since the photodecomposition of the complex depends strongly on the availability of UV radiation and would be implemented through a proper control system. It is important to remark the agreement between the model and the experimental results when the irradiation changed, indicating the consistency of the model.

In the 15-cm RPR, the Fe^{3+}-EDDS conversion is slightly overestimated. This could be due to the geometrical proportions of the 15-cm RPR are different from those of the 5-cm RPR (5.1 vs 2.4 length of the straight section of the reactor: channel width), and the kinetics parameters were previously determined from the data obtained in the 5-cm RPR. Even so, the model successfully predicts the H_2O_2 consumption and CEC removal.

4.2. Effect of HRT and liquid depth on the treatment capacity

In RPRs, liquid depth can be varied, and consequently, the treatment capacity, according to the availability of UV radiation. Therefore, liquid depth could be tuned according to solar irradiance, if needed.

Simulation of the continuous flow operation of the RPR was carried out as a function of HRT and liquid depth both in winter and summer clear day solstices, which correspond to the days with the lowest and highest hours of sunlight, respectively. To simplify the presentation of results and better understand the application of the developed model to the continuous operation, the hours in the day at which the global UV radiation is ≥ 10 W m^{-2} were set as total hours of operation [14], 4.5 h in winter solstice (December 21st) and 10 h in summer solstice (June 21st).

Table 5 shows the effect of HRT as a function of liquid depth in winter and summer solstices on the removal of the selected CECs (with respect to the sum of the three CECs). The contribution of the dark Fenton reactions is also shown, reaching CEC removal as high as 57% at 30-min HRT. Nonetheless, the treatment target should be significantly higher, around 80% [3]. Furthermore, the Fe^{3+}-EDDS is the limiting reactant and the most expensive. Therefore, for economic purposes, high Fe^{3+}-EDDS conversions are desirable. These goals can only be attained by the Fenton process but at so long and not realistic HRT for any application.

In winter solstice, the 81% CEC removal is estimated at 30-min HRT in 5-cm deep RPRs. Accordingly, the treatment capacity would be 450 L m^{-2} d^{-1}. Under these conditions, the conversion of the Fe^{3+}-EDDS complex is 77%. As for summer solstice, several combinations of HRT

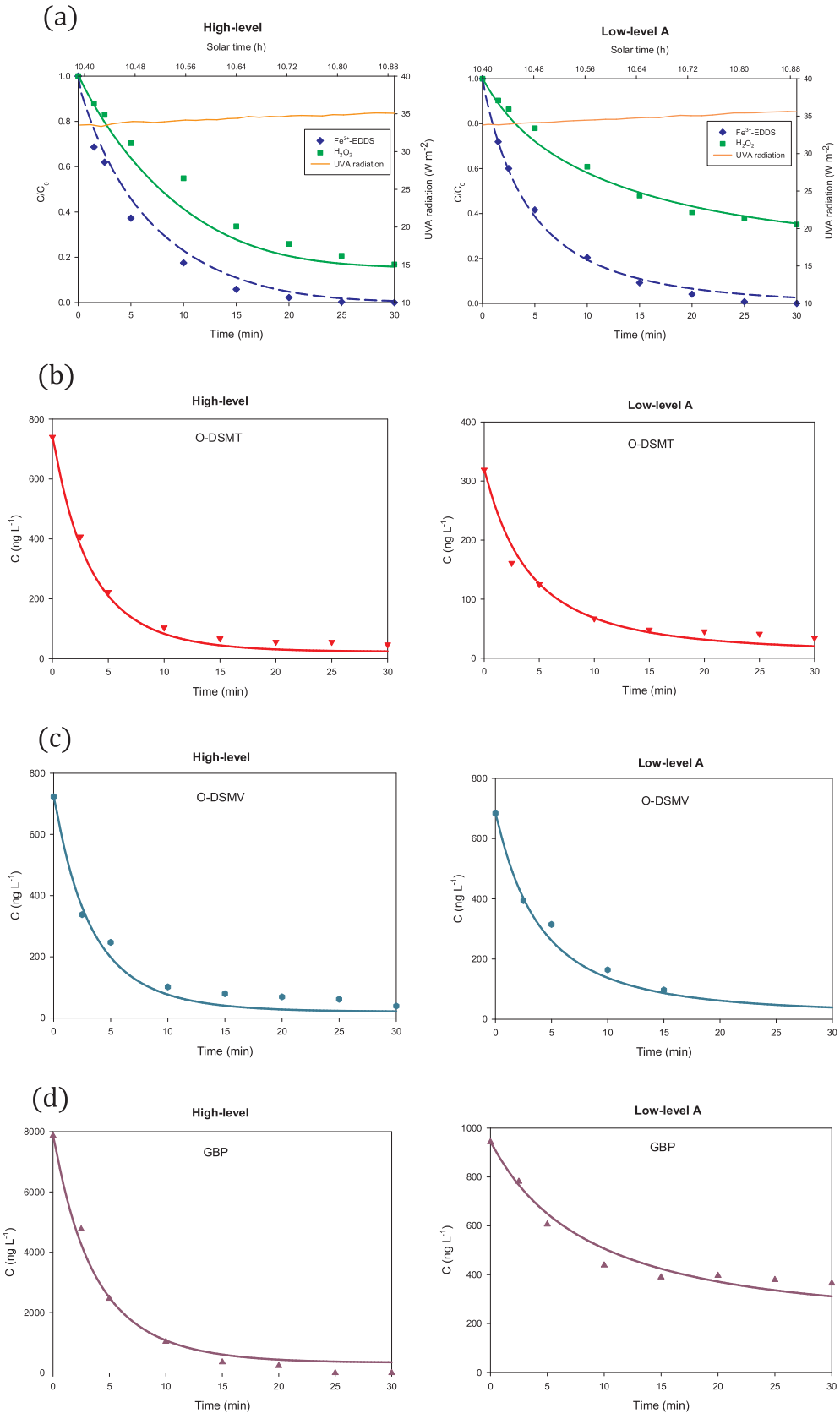

Fig. 2. Fe^{3+}-EDDS, H_2O_2 (a), *O*–DSMT (b), *O*–DSMV (c) and GBP (d) profiles in high-level and low-level A effluents. Lines represent model estimations.

Table 4
Dynamic model equations for continuous flow operation.

Mass balance model states	Equation number
$\frac{d[[Fe^{3+}-EDDS]^-]}{dt} = \frac{Q_F}{V}[Fe^{3+} - EDDS]^-_e - \frac{Q_S}{V}[Fe^{3+} - EDDS]^- - r_1 + r_2 + r_4 - r_7 - r_8$	Eq. (3)
$\frac{d[[Fe^{3+}-EDDS]^{-*}]}{dt} = -\frac{Q_S}{V}[Fe^{3+} - EDDS]^{-*} + r_1 - r_2 - r_3$	Eq. (4)
$\frac{d[Fe^{2+}]}{dt} = -\frac{Q_S}{V}[Fe^{2+}] + r_5 - r_6 + r_{11}$	Eq. (5)
$\frac{d[Fe^{2+}-EDDS]}{dt} = -\frac{Q_S}{V}[Fe^{2+} - EDDS] + r_3 - r_4 - r_5 + r_7$	Eq. (6)
$\frac{d[Fe^{3+}-EDDSox]}{dt} = -\frac{Q_S}{V}[Fe^{3+} - EDDSox] + r_8 - r_9 + r_{10}$	Eq. (7)
$\frac{d[[Fe^{3+}-EDDSox]^*]}{dt} = -\frac{Q_S}{V}[Fe^{3+} - EDDSox]^* + r_9 - r_{10} - r_{11}$	Eq. (8)
$\frac{d[H_2O_2]}{dt} = \frac{Q_H}{V}[H_2O_2]_e - \frac{Q_S}{V}[H_2O_2] - r_4 - r_6 - r_7 - r_{14} - r_{15}$	Eq. (9)
$\frac{d[HO^\bullet]}{dt} = -\frac{Q_S}{V}[HO^\bullet] + r_4 + r_6 - r_8 - r_{12} - r_{13} - r_{14} - r_{16} - r_{17} - r_{18}$	Eq. (10)
$\frac{d[OM^a]}{dt} = \frac{Q_W}{V}[OM^a]_e - \frac{Q_S}{V}[OM^a] - r_{12}$	Eq. (11)
$\frac{d[MX^b]}{dt} = -\frac{Q_S}{V}[MX^b] + r_{12} + 10\,r_{15} + 15\,r_{16} + 16\,r_{17} + 9\,r_{18}$	Eq. (12)
$\frac{d[IC^c]}{dt} = \frac{Q_W}{V}[IC^c]_e - \frac{Q_S}{V}[IC^c] - r_{13}$	Eq. (13)
$\frac{d[ICX^d]}{dt} = -\frac{Q_S}{V}[ICX^d] + r_{13}$	Eq. (14)
$\frac{d[EDDS^{\bullet 3-}]}{dt} = -\frac{Q_S}{V}[EDDS^{\bullet 3-}] + r_5 + r_{11} - r_{15}$	Eq. (15)
$\frac{d[O-DSMT^e]}{dt} = \frac{Q_W}{V}[O-DSMT^e]_e - \frac{Q_S}{V}[O-DSMT^e] - r_{16}$	Eq. (16)
$\frac{d[O-DSMV^f]}{dt} = \frac{Q_W}{V}[O-DSMV^f]_e - \frac{Q_S}{V}[O-DSMV^f] - r_{17}$	Eq. (17)
$\frac{d[GBP^g]}{dt} = \frac{Q_W}{V}[GBP^g]_e - \frac{Q_S}{V}[GBP^g] - r_{18}$	Eq. (18)

[a]Organic matter; [b]Oxidized organic matter; [c]Inorganic carbon; [d]Oxidized inorganic carbon; [e]*O*-Desmethyltramadol; [f]*O*-Desmethylvenlafaxine; [g]Gabapentin.

and liquid depth give rise to CEC removal > 80%. The shortest HRT is 15 min with 5 cm of liquid depth, giving 2000 L m^{-2} d^{-1} of treatment capacity, and it could be doubled (4000 L m^{-2} d^{-1}) by increasing at the same time both the HRT and the liquid depth to 30 min and 20 cm, respectively. In all cases, the Fe^{3+}-EDDS conversion is above 76%.

On the other hand, the range of operation depends on the targeted removal of CECs as shown by the colored areas in Table 5 and Fig. 4, which show the treatment capacity to achieve a target percentage of CEC removal as a function of the liquid depth and the HRT. As it can be observed, a higher target of removal would imply a less flexible operating range in terms of liquid depth and HRT. Furthermore, at a specific HRT, the treatment capacity achieved in winter solstice is much lower than in summer solstice, in concordance with the greater availability of solar radiation. In winter solstice, 15-min HRT would be enough to achieve 70% degradation at short liquid depths of 5 cm, the treatment capacity being 900 L m^{-2} d^{-1}, point A in Fig. 4a. In summer, the HRT could be hafted using 5 cm, giving rise to 4000 L m^{-2} d^{-1} treatment capacity, point B in Fig. 4b, or extended to 20 min with 30-cm liquid depth, the treatment capacity being increased to 9000 L m^{-2} d^{-1}, point C in Fig. 4b.

Of course, simulations were done using two extreme situations (winter and summer solstices) and therefore the treatment capacity would change along the year between 900 and 9000 L m^{-2} d^{-1} permitting a smooth operation by a proper and simple control of HRT and liquid depths. The objective would be to maximize the treatment capacity in a day by day basis.

These simulation results are useful for RPR design on a larger scale, since the reactor area, which is the main parameter for photoreactor design and investment costs, could be estimated given the daily flow rate and the target removal percentage (Fig. 4). As an example, to treat 400 m^3 d^{-1} [30] and remove 80% CECs in winter solstice, 5-cm liquid depth and 30-min HRT would be required to achieve the highest treatment capacity (450 L m^{-2} d^{-1}), an RPR area of 888 m^2 being estimated. In summer solstice, 20 cm liquid depth and 30 min HRT would be required to achieve the highest treatment capacity (4000 L m^{-2} d^{-1}) an RPR area of 100 m^2 being estimated. Furthermore, the final reactor design strongly depends on fluid-dynamics and mixing. When conducting the process with Fe^{3+}-EDDS, the reactor should be operated in turbulent flow to reduce mixing time. In this regard, energy consumption necessary for strong mixing in RPRs is fundamental. It should be noticed that this energy consumption would not imply high energy costs, since the unitary power requirement for mixing in RPRs is low, over 4 W m^{-3} [31]. Indeed, the energy cost of the operation of RPRs in continuous flow mode is estimated to be only 6% of operating cost [12].

5. Conclusions

A designing tool for wastewater treatment in RPRs is proposed. The kinetic parameters of photo-Fenton model developed with synthetic effluent were slightly tuned to predict CEC removal in real MWWTP effluents. The model is able to predict both the reactant consumption and CEC removal when operating RPRs with different liquid depths in continuous flow mode. In these conditions, it is possible to achieve a high conversion (> 80%) at short reaction times (in the range 10–30 min) when performing the process at neutral pH with Fe^{3+}-EDDS (not stable at long reaction times). Simulations showed that 80% CEC removal can be achieved at 30-min HRT in 5-cm deep RPRs in winter solstice, the treatment capacity (supposing 4.5 h of operation per day) being 450 L m^{-2} d^{-1}, and it could be increased up to 4000 L m^{-2} d^{-1} in summer solstice (supposing 10 h of operation per day), increasing the liquid depth by four times. In both conditions, high Fe^{3+}-EDDS conversions of around 80% were estimated. The results presented are of relevance for RPR design, since for a given target CEC removal, the reactor area could be estimated as a function of the hydraulic HRT and liquid depth. This maximizes the treatment capacity as a function of solar irradiation conditions.

Acknowledgements

The authors would like to acknowledge the Ministry for Economy,

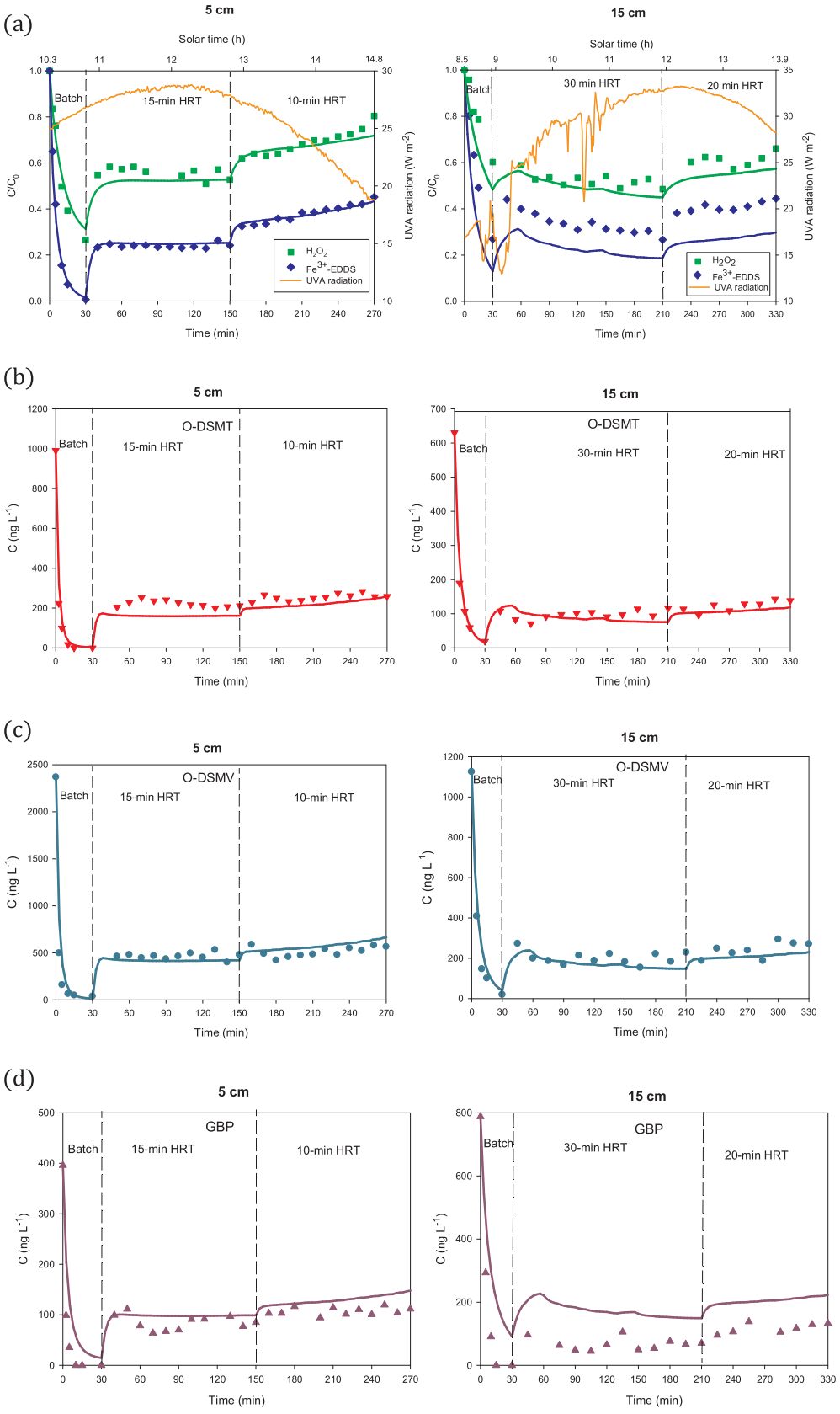

Fig. 3. Model validation in 5-cm and 15-cm deep RPRs operated in continuous flow mode: (a) Fe^{3+}-EDDS and H_2O_2, (b) O-DSMT, (c) O-DSMV, (d) GBP. Solid lines represent model predictions.

Table 5
Effect of hydraulic residence time (HRT) on CEC removal as a function of liquid depth in winter and summer solstices. Green, blue and red areas correspond to 60, 70 and 80% CEC removal, respectively.

HRT (min)	CEC removal (%)										
		Winter					Summer				
	Fenton	Liquid depth (cm)									
		5	10	15	20	30	5	10	15	20	30
5	28	51	44	41	38	36	62	55	50	47	42
7.5	34	59	53	49	46	43	70	64	59	56	51
10	39	65	59	55	52	49	74	69	65	62	57
12.5	43	68	63	59	57	53	77	73	70	66	61
15	46	71	66	63	60	57	80	76	73	70	65
20	51	76	71	68	65	62	83	80	77	75	70
25	55	78	75	72	69	66	85	83	80	78	74
30	57	81	77	74	72	69	86	85	83	81	77

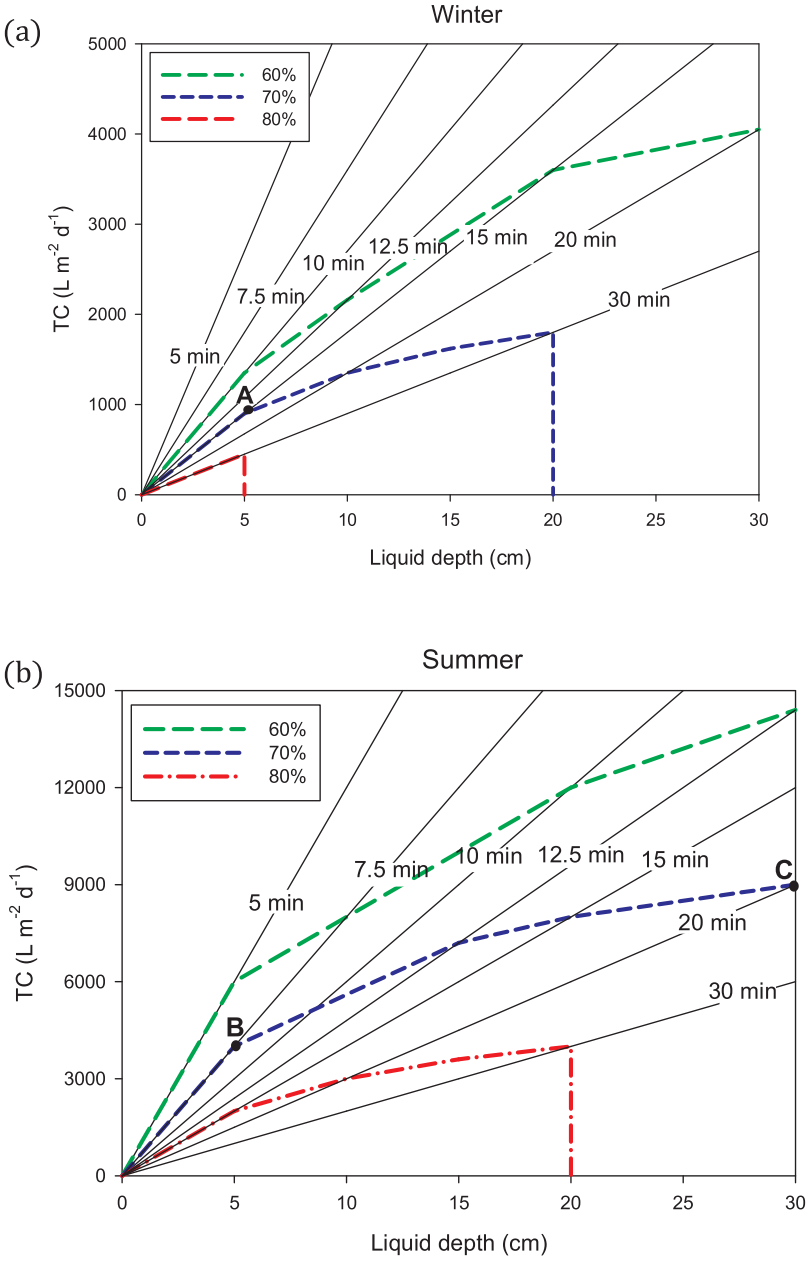

Fig. 4. Model estimation of treatment capacity, TC, in winter solstice (a) and summer solstice (b) as a function of liquid depth with the HRT as a parameter (lines). The area inside the dashed lines represents operating range to achieve a target percentage of CEC removal.

Industry and Competitiveness (Spanish Government) and the European Regional Development Fund (ERDF), project CTQ2016-78255-R. P. Soriano-Molina is grateful to the Ministry of Education, Culture and Sport for her FPU scholarship (AP2014/01030). P. Plaza-Bolaños would like to acknowledge the University of Almeria for her research contract (Hypatia Program).

Appendix A. Supplementary data

Supplementary material related to this article can be found, in the online version, at doi:https://doi.org/10.1016/j.apcatb.2019.117801.

References

[1] M. Salimi, A. Esrafili, M. Gholami, A. Jonidi Jafari, R. Rezaei Kalantary, M. Farzadkia, M. Kermani, H.R. Sobhi, Contaminants of emerging concern: a review of new approach in AOP technologies, Environ. Monit. Assess. 189 (2017) 414, https://doi.org/10.1007/s10661-017-6097-x.

[2] E.A. Serna-Galvis, A.M. Botero-coy, D. Martínez-Pachón, A. Moncayo-Lasso, M. Ibáñez, R.A. Torres-Palma, Degradation of seventeen contaminants of emerging concern in municipal wastewater effluents by sonochemical advanced oxidation processes, Water Res. 154 (2019) 349–360, https://doi.org/10.1016/j.watres.2019.01.045.

[3] Waters Protection Ordinance of 28 October 1998 (814.201) (Status of 1 June 2018), (2018) https://www.admin.ch/opc/en/classifiedcompilation/19983281/index.html.

[4] J.C.G. Sousa, A.R. Ribeiro, M.O. Barbosa, C. Ribeiro, M.E. Tiritan, M.F.R. Pereira, A.M.T. Silva, Monitoring of the 17 EU watch list contaminants of emerging concern in the Ave and the Sousa rivers, Sci. Total Environ. 649 (2019) 1083–1095, https://doi.org/10.1016/j.scitotenv.2018.08.309.

[5] L. Rizzo, S. Malato, D. Antakyali, V.G. Beretsou, M.B. Đolić, W. Gernjak, E. Heath, I. Ivancev-Tumbas, P. Karaolia, A.R. Lado Ribeiro, G. Mascolo, C.S. McArdell, H. Schaar, A.M.T. Silva, D. Fatta-Kassinos, Consolidated vs new advanced treatment methods for the removal of contaminants of emerging concern from urban wastewater, Sci. Total Environ. 655 (2019) 986–1008, https://doi.org/10.1016/j.scitotenv.2018.11.265.

[6] R. Ameta, A.K. Chohadia, A. Jain, P.B. Punjabi, S.C. Ameta, R. Ameta (Eds.), Advanced Oxidation Processes for Wastewater Treatment: Emerging Green Chemical Technology, Academic Press, 2018, pp. 49–87, , https://doi.org/10.1016/B978-0-12-810499-6.00003-6.

[7] N. Diaz-Elsayed, N. Rezaei, T. Guo, S. Mohebbi, Q. Zhang, Wastewater-based resource recovery technologies across sclae: a review, Resour Conserv. Recy 145 (2019) 94–112, https://doi.org/10.1016/j.resconrec.2018.12.035.

[8] L. Clarizia, D. Russo, I. Di Somma, R. Marotta, R. Andreozzi, Homogeneous photo-Fenton processes at near neutral pH: a review, Appl. Catal. B: Environ. 209 (2017) 358–371, https://doi.org/10.1016/j.apcatb.2017.03.011.

[9] S. Papoutsakis, S. Miralles-Cuevas, I. Oller, J.L. Garcia Sanchez, C. Pulgarin, S. Malato, Microcontaminant degradation in municipal wastewater treatment plant secondary effluent by EDDS assisted photo-Fenton at near-neutral pH: an experimental design approach, Catal. Today 252 (2015) 61–69, https://doi.org/10.1016/j.cattod.2015.02.005.

[10] E. Cuervo Lumbaque, D. Salmoria Araújo, T. Moreira Klein, E.R. Lopes Tiburtius, J. Argüello, C. Sirtori, Solar photo-Fenton-like process at neutral pH: Fe(III)-EDDS complex formation and optimization of experimental conditions for degradation of pharmaceuticals, Catal. Today 328 (2019) 259–266, https://doi.org/10.1016/j.cattod.2019.01.006.

[11] P. Soriano-Molina, J.L. García Sánchez, S. Malato, L.A. Pérez-Estrada, J.A. Sánchez Pérez, Effect of volumetric rate of photon absorption on the kinetics of micropollutant removal by solar photo-Fenton with Fe3 + -EDDS at neutral pH, Chem. Eng. J. 331 (2018) 84–92, https://doi.org/10.1016/j.cej.2017.08.096.

[12] P. Soriano-Molina, P. Plaza-Bolaños, A. Lorenzo, A. Agüera, J.L. García Sánchez, S. Malato, J.A. Sánchez Pérez, Assessment of solar raceway pond reactors for removal of contaminants of emerging concern by photo-Fenton at circumneutral pH from very different municipal wastewater effluents, Chem. Eng. J. 366 (2019) 141–149, https://doi.org/10.1016/j.cej.2019.02.074.

[13] G. Rivas Ibáñez, M. Bittner, Z. Toušová, M.C. Campos-Mañas, A. Agüera, J.L. Casas López, J.A. Sánchez Pérez, K. Hilscherová, Does micropollutant removal by solar photo-Fenton reduce ecotoxicity in municipal wastewater? A comprehensive study at pilot scale open reactors, J. Chem. Technol. Biotechnol. 92 (2017) 2114–2122, https://doi.org/10.1002/jctb.5212.

[14] A. Cabrera Reina, J.L. Casas Liópez, M.I. Maldonado Rubio, L. Santos-Juanes Jordá, J.L. Garcia Sanchez´, J.A. Sánchez Pérez, Effects of environmental variables on the photo-Fenton plant design, Chem. Eng. J. 237 (2014) 469–477, https://doi.org/10.1016/j.cej.2013.10.046.

[15] A.V. Schenone, L.O. Conte, M.A. Botta, O.M. Alfano, Modeling and optimization of photo-Fenton degradation of 2,4-D using ferrioxalate complex and response surface methodology (RSM), J. Environ. Manage. 155 (2015) 177–183, https://doi.org/10.1016/j.jenvman.2015.03.028.

[16] S. Giannakis, I. Hendaoui, S. Rtimi, J. Fürbringer, C. Pulgaría, Modeling and treatment optimization of pharmaceutically active compounds by the photo-Fenton process: the case of the antidepressant venlafaxine, J. Environ. Chem. Eng. 5 (2017) 818–828, https://doi.org/10.1016/j.jece.2016.12.050.

[17] P. Soriano-Molina, J.L. García Sánchez, O.M. Alfano, L.O. Conte, S. Malato, J.A. Sánchez Pérez, Mechanistic modeling of solar photo-Fenton process with Fe^{3+}-EDDS at neutral pH, Appl. Catal. B: Environ. 233 (2018) 234–242, https://doi.org/10.1016/j.apcatb.2018.04.005.

[18] E.M. Siedlecka, P. Stepnowski, Decomposition rates of methyl tert-butyl ether and its by-products by the Fenton system in saline wastewaters, Sep. Purif. Technol. 52 (2006) 317–324, https://doi.org/10.1016/j.seppur.2006.05.014.

[19] A.R. Lado Ribeiro, N.F.F. Moreira, G. Li Puma, A.M.T. Silva, Impact of water matrix on the removal of micropollutants by advanced oxidation technologies, Chem. Eng. J. 363 (2019) 155–173, https://doi.org/10.1016/j.cej.2019.01.080.

[20] M. Herrmann, J. Menz, O. Olsson, K. Kümmerer, Identification of photo-transformation products of the antiepileptic drug gabapentin: biodegradability and initial assessment of toxicity, Water Res. 85 (2015) 11–21, https://doi.org/10.1016/j.watres.2015.08.004.

[21] P.C. Rúa-Gómez, W. Püttmann, Degradation of lidocaine, tramadol, venlafaxine and the metabolites O-desmethyltramadol and O-desmethylvenlafaxine in surface waters, Chemosphere 90 (2013) 1952–1959, https://doi.org/10.1016/j.chemosphere.2012.10.039.

[22] N.F.F. Moreira, M.J. Sampaio, A.R. Ribeiro, C.G. Silva, J.L. Faria, A.M.T. Silva, Metal-free g-C3N4 photocatalysis of organic micropollutants in urban wastewater under visible light, Appl. Catal. B: Environ. 248 (2019) 184–192, https://doi.org/10.1016/j.apcatb.2019.02.001.

[23] M.C. Campos-Mañas, I. Ferrer, E.M. Thurman, A. Agüera, Opioid occurrence in environmental water samples—a review, Trends Environ. Anal. 20 (2018) e00059, , https://doi.org/10.1016/j.teac.2018.e00059.

[24] Y. Wu, M. Brigante, W. Dong, P. De Sainte-Claire, G. Mailhot, Toward a better understanding of Fe(III)–EDDS photochemistry: theoretical stability calculation and experimental investigation of 4-tert-butylphenol degradation, J. Phys. Chem. A 118 (2014) 396–403, https://doi.org/10.1021/jp409043e.

[25] M.C. Campos-Mañas, P. Plaza-Bolaños, J.A. Sánchez-Pérez, S. Malato, A. Agüera, Fast determination of pesticides and other contaminants of emerging concern in treated wastewater using direct injection coupled to highly sensitive ultra-high performance liquid chromatography-tandem mass spectrometry, J. Chromatogr. A 1507 (2017) 84–94, https://doi.org/10.1016/j.chroma.2017.05.053.

[26] A. Belalcázar-Saldarriaga, D. Prato-García, R. Vasquez-Medrano, Photo-Fenton processes in raceway reactors: technical, economic, and environmental implications during treatment of colored wastewaters, J. Clean. Prod. 182 (2018) 818–829, https://doi.org/10.1016/j.jclepro.2018.02.058.

[27] C. Gueymard, SMARTS2, a Simple Model of the Atmospheric Radiative Transfer of Sunshine: Algorithms and Performance Assessment. Rep. FSEC-PF-270-95, Florida Solar Energy Center, Cocoa, USA, 1995.

[28] G.V. Buxton, C.L. Greenstock, W.P. Helman, A.B. Ross, Critical review of rate constants for reactions of hydrated electrons, hydrogen atoms and hydroxyl radicals (•OH/O −) in aqueous solution, J. Phys. Chem. Ref. Data 17 (1988) 513–886, https://doi.org/10.1063/1.555805.

[29] R. Chen, J.J. Pignatello, Role of quinone intermediates as Electron shuttles in Fenton and photoassisted Fenton oxidations of aromatic compounds, Environ. Photochem. 31 (1997) 2399–2406, https://doi.org/10.1021/es9610646.

[30] Council Directive of 21 May 1991 Concerning Urban Waste Water Treatment (91/271/EEC), (1991), pp. 40–52 Off. J. L 135, 30.5.1991 https://eur-lex.europa.eu/eli/dir/1991/271/oj.

[31] I. Carra, L. Santos-Juanes, F.G. Acién Fernández, S. Malato, J.A. Sánchez Pérez, New approach to solar photo-Fenton operation. Raceway ponds as tertiary treatment technology, J. Hazard. Mater. 279 (2014) 322–329, https://doi.org/10.1016/j.jhazmat.2014.07.010.